Trinitrophenylated Reactive Lysine Residue in Myosin Detects Lever Arm Movement during the Consecutive Steps of ATP Hydrolysis†

Katalin Ajtai,‡ Y. Michael Peyser,§ Sungjo Park,‡ Thomas P. Burghardt,*,‡ and Andras Muhlrad§

Department of Biochemistry and Molecular Biology, Mayo Foundation, Rochester, Minnesota 55905, and Department of Oral Biology, Hebrew University-Hadassah School of Dental Medicine, Jerusalem, Israel 91120

Received January 21, 1999; Revised Manuscript Received March 17, 1999

ABSTRACT: Trinitrophenylation of the reactive lysine (Lys84) in skeletal myosin subfragment 1 (S1) introduces a chiral probe (TNP) into an interface of the catalytic and lever arm domains of S1 [Muhlrad (1977) *Biochim. Biophys. Acta 493,* 154−166]. Characteristics of the TNP absorption and circular dichroism (CD) spectra in TNP-modified S1 (TNP-Lys84-S1), and the Lys84 trinitrophenylation rate in native S1, indicate a one-to-one correspondence between ATPase transients and trapped phosphate analogues. Phosphate analogue-induced structures of TNP-Lys84-S1 were modeled using the crystallographic coordinates of S1 [Rayment et al. (1993) *Science 261,* 50−58] with swivels at Gly699 and Gly710 to approximate conformational changes during ATPase. The CD and absorption spectral characteristics of the model structures were compared to those observed for analogue-induced structures. The model calculations, first tested on a trinitrophenylated hexapeptide with known structure, were applied to TNP-Lys84-S1. They showed that ATP binding initiates swiveling at Gly699 and that swiveling at both Gly710 and Gly699 accompanied ATP splitting just prior to product release. The computed lever arm trajectory during ATPase suggests (i) a plausible mechanism for the nucleotide-induced inhibition of Lys84 trinitrophenylation, and (ii) trinitrophenylation-induced changes in S1 Mg^{2+}- and K^{+}-EDTA ATPase are from collision of the lever arm with TNP at Lys84. TNP is a site-specific structural perturbant of S1 and a chiral reporter group for the effect of Lys84 modification on dynamic S1 structure. As such, TNP-Lys84-S1 is equivalent to a genetically engineered mutant with intrinsic sensitivity to structure local to the modified residue.

Myosin is the most abundant and important motor protein in nature. Its interaction with actin coupled with ATP hydrolysis is the molecular basis of muscle contraction and has also an important role in the motility of nonmuscle eukaryotic cells. The globular head of myosin, called subfragment 1 or S1,[1] where both the nucleotide- and actin-binding sites of the molecule are located, is responsible for the generation of force during contraction. According to the simplified scheme of Bagshaw and Trentham (*1*) the myosin-catalyzed ATP hydrolysis consists of the consecutive steps

Scheme 1

$$M + ATP \overset{1}{\leftrightarrow} M^{*}\cdot ATP \overset{2}{\leftrightarrow} M^{**}\cdot ADP\cdot Pi \overset{3}{\leftrightarrow} M^{*}\cdot ADP + Pi \overset{4}{\leftrightarrow} M + ADP + Pi$$

where M is myosin and M, M*·ATP, M**·ADP·Pi, and M*·ADP represent conformational states of myosin−nucleotide complexes with distinct spectral properties.

The conformational changes taking place during the transitions between the ATP hydrolysis intermediates alter myosin's actin affinity and cause the relative sliding of myosin and actin filaments during force generation. One scheme for producing filament movement has a weakly actin bound cross-bridge hydrolyzing ATP, forming a strong link to actin, then delivering the impulsive force when it releases product and returns to the low free energy no bound nucleotide conformation. In this scheme, the rotating cross-bridge model of contraction has the cross-bridge rotating after strong actin binding to develop torque and deliver the impulsive force to the actin filament (*2*, *3*).

The site of torque generation has been proposed to reside in a converter region within the cross-bridge at the interface of a fixed globular catalytic/actin-binding domain and a rotating lever arm domain based on analogy with adenylate kinase (*4*). Two conserved glycine residues in S1, Gly699, and Gly710 are essential for function and suggested to be pivots in the converter region peptide backbone, facilitating lever arm movement in the cross-bridge (*5*, *6*). Consistent with this picture are certain spectroscopic signals related to

† This work was supported by the National Institutes of Health Grant R01 AR39288 and the Mayo Foundation.

* To whom correspondence should be addressed.

‡ Mayo Foundation.

§ Hebrew University-Hadassah School of Dental Medicine.

[1] Abbreviations: AlF_4^-, aluminum fluoride complex; ATPγS, adenosine-5′-*O*-3-thiotriphosphate; BeF_x, beryllium fluoride complex; CD, circular dichroism; DMSO, dimethyl sulfoxide; *N*-acetyl-PPKYDK-NH_2, model peptide sequence named 6p; PA, phosphate analogue; PPi, pyrophosphate; Pi, inorganic phosphate; RLR, reactive lysyl residue or Lys84 (Lys83 in rabbit skeletal myosin); S1, myosin subfragment 1; S1Dc, truncated Dictyostelium S1; SH1, most reactive thiol or Cys707; TNBS, 2,4,6-trinitrobenzene sulfonate; TNP, trinitrophenyl; UV, ultra violet; Vi, vanadate. Myosin sequence numeration that of skeletal chicken.

10.1021/bi990149r CCC: $18.00
Published on Web 04/29/1999

the conformation of the probe-binding cleft containing the reactive thiol, Cys707, and an ATP-sensitive tryptophan, Trp510. Pivoting the peptide backbone at Gly699 causes conformation changes in the probe-binding cleft affecting quencher accessibility (*7*, *8*), the circular dichroism (CD) of Trp510 (*9*), and lever arm position (*10*). Furthermore, the crystal structure of smooth muscle S1 with active site trapped by MgADP·AlF_4^- identified Gly699 and Gly710 as functional pivots (*11*).

Evidently, for understanding the mechanism of energy transduction and force generation in the actomyosin motor, it is essential to establish the conformation of the myosin head during ATP hydrolysis and product release. Although the myosin ATPase intermediates are short-lived making their structure determination difficult, the analogues of the γ-phosphate (Pi)—vanadate (Vi), beryllium fluoride (BeF_x), and aluminum fluoride (AlF_4^-) complexes—remedy this difficulty by substituting Pi and trapping the myosin in its transient structure (*12*−*14*). The complexes of the recombinant truncated Dictyostelium S1 (S1Dc) with BeF_x, AlF_4^-, and Vi—S1Dc·ADP·BeF_x, S1Dc·ADP·AlF_4^-, S1Dc·ADP·Vi—were recently crystallized and their structures solved (*15*, *16*). These studies have shown significant structural differences between the complexes and indicated that S1Dc·ADP·BeF_x resembles the M*·ATP while S1Dc·ADP·AlF_4^- and S1Dc·ADP·Vi mimic the M**·ADP·Pi intermediate state.

Several solution studies using EPR, NMR, and fluorescence techniques also showed differences among the structures of the various stable S1-nucleotide-phosphate analogue (PA) complexes (*8*, *14*, *17*, *18*). The results of near-UV CD (*19*) and most reactive thiol (SH1 or Cys707) modification kinetics (*20*) measurements supported the conclusions of the crystallography about the resemblance of the stable S1-nucleotide-PA complexes to the specific transient states of the ATP hydrolysis. More precisely, these studies indicated that the structures of the stable complexes are similar but not identical to the structures of the real ATPase intermediates. We use here PA-containing stable complexes and chemical modification of a reactive lysine residue to probe the structural intermediates of myosin during ATPase.

Lys84 is the most reactive lysine residue of the myosin head (*21*) located in the 27kDa N-terminal segment of the molecule (*22*, *23*) at an interface of the catalytic and lever arm domains (Figure 1) not too near the active site (*4*). Its rate of trinitrophenylation with trinitrobenzene sulfonate (TNBS) to form TNP-Lys84-S1 is 3 orders of magnitude faster than the rest of the lysine residues (*24*) but strongly inhibited by ATP and ATP analogues (*25*). Lys84 trinitrophenylation causes a 20-fold increase in Mg^{2+}, and a 10-fold decrease in K^+-EDTA, ATPase activity of S1 (*26*, *27*). As a consequence of modification of Lys84, the M*·ATP state becomes the predominant intermediate of the ATPase cycle (*28*). The TNP in TNP-Lys84-S1 has a characteristic CD spectrum that is strongly affected by ATP and ATP analogues and an absorbance spectrum that is also sensitive to nucleotides and shows a blue shift in their presence (*29*). These findings indicate that the region of S1 local to Lys84 communicates with the active site of myosin. In this manuscript we describe experiments and calculations using TNP-modified Lys84 in S1 to elucidate the structural similarities between PA-containing complexes and comparable states of the ATP hydrolysis and the mechanism-sensitizing TNP to nucleotide hydrolysis in the active site.

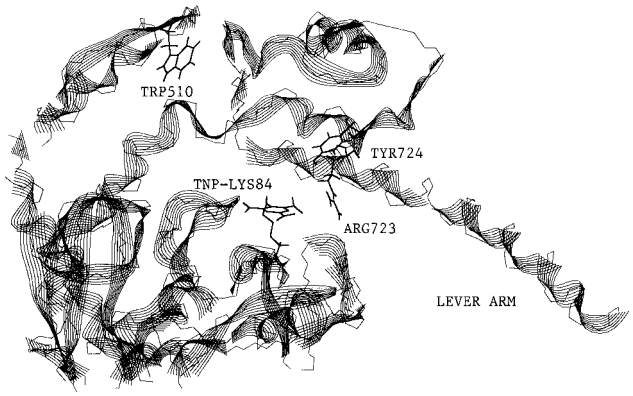

FIGURE 1: S1 trinitrophenylated at Lys84 and showing the interface of the catalytic and lever arm domains at the probe-binding cleft (containing Trp510) and at Lys84. The main α-helix of the S1 separates the probe-binding cleft from the TNP-Lys84. The TNP is in close proximity to Arg723 in this overview representing S1 structure in the absence of nucleotide.

We studied the effect of ATP, ADP, ADP·BeF_x, ADP·AlF_4^-, ADP·Vi, and ATPγS (ATPγS forms a complex with S1 mimicking the M*·ATP state (*30*)) on the rate of trinitrophenylation of S1 and on the CD and absorbance spectra of the TNP in TNP-Lys84-S1. In agreement with the crystallographic studies, conformation in the vicinity of Lys84 in the S1·ADP·AlF_4^- and S1·ADP·Vi complexes resembles that in M**·ADP·Pi while S1·ADP·BeF_x resembles that in the M*·ATP intermediate.

We compared the peak energy, dipole, and rotary strengths from the observed absorption and CD signals at the two lowest energy electronic transitions of TNP in TNP-Lys84-S1 with theoretical values computed for these transitions using methods described previously (*10*). The calculation methods were first tested on a trinitrophenylated hexapeptide with structure determined by 2D-NMR and shown to accurately reproduce the observed spectroscopic characteristics of the hexapeptide. Calculated values for TNP-Lys84-S1, based on the crystallographic structure of skeletal S1 (*4*) with pivoting at Gly699 and Gly710 to model myosin structural changes accompanying the formation of stable PA complexes, quantitatively accounted for all of the observed spectroscopic characteristics of the TNP-Lys84-S1. In all cases the position of Tyr85 relative to TNP strongly influences the optical activity of the probe. In the absence of nucleotide analogues, the model calculations suggest that the proximity of Tyr724 strongly influences the optical activity of the probe while an electrostatic interaction with Arg723 immobilizes TNP in TNP-Lys84-S1 (Figure 1). Swiveling only at Gly699 accompanies the M → M*·ATP transition while the TNP maintains proximity to Tyr724 and an interaction with Arg723. Swiveling at both Gly710 and Gly699 accompanies the M*·ATP → M**·ADP·Pi transition removing Tyr724 and Arg723 from the vicinity of TNP but allowing formation of a TNP-Tyr85 hydrogen bond to constrain TNP mobility. During the M*·ATP → M**·ADP·Pi transition the lever arm collides with TNP, possibly interfering with the formation and stability of the M**·ADP·Pi intermediate.

MATERIALS AND METHODS

Chemicals. ATP, ADP, $BeCl_2$ (dissolved in 1% HCl), α-chymotrypsin, dimethyl sulfoxide (DMSO), dithioerythritol, HEPES, *N*-acetyl-L-lysine, phenylmethane sulfonyl fluoride, and Tris-HCl were from Sigma (St. Louis, MO). TNBS was from Fluka (Milwaukee, WI). ATPγS was purchased from Boehringer Mannheim (Indianapolis, IN). All other chemicals were reagent grade. A stock solution of sodium vanadate (100 mM) was prepared according to Goodno (*12*). NaF stock solutions were freshly prepared daily.

Peptide Synthesis. A model peptide, with the sequence *N*-acetyl-PPKYDK-NH_2 (6p) taken from chicken S1 sequence surrounding Lys84, was synthesized and specifically modified with TNP at Lys3 (TNP-6p) by the Mayo Protein Core Facility. Two-dimensional nuclear magnetic resonance (2D-NMR) was used to determine the peptide structure (*31*).

Preparation of Proteins. Myosin was prepared from back and leg muscles of rabbit by the method of Tonomura et al. (*32*). S1 was obtained by digestion of myosin filaments with α-chymotrypsin as described by Weeds and Taylor (*33*). Protein concentrations were obtained by absorbance, using an *A*(1%) at 280 nm of 5.5 and 7.5 for myosin and S1, respectively. Molecular masses were assumed to be 500 and 115 kDa for myosin and S1, respectively.

Chemical Modification. S1 was trinitrophenylated, if not stated otherwise, by the addition of 2-fold molar excess TNBS to 60−80 μM S1 in 30 mM KCl and 100 mM Tris HCl buffer, pH 7.8. After incubation at 25 °C for 10 min the reaction was terminated by the addition of 2 mM dithioerythritol. Excess TNBS was removed by dialyzing at least twice against 100 volumes of 1 mM dithioerythritol, 30 mM KCl, and 30 mM HEPES buffer, pH 7.0 at 4 °C (no dithioerythritol in final dialysis). The number of TNP groups introduced was obtained from absorbance at 345 nm using $\epsilon_{345} = 14\,500\ (\mathrm{M\ cm})^{-1}$ according to Okuyama and Satake (*34*). For calculation of TNP-modified S1 concentration the absorbance at 280 nm was corrected according to the following formula: corrected(A_{280}) = observed(A_{280}) − (0.362)observed(A_{345}). S1 modified by TNBS under these circumstances had a (mole of TNP)/(mole of S1) ratio of 1 with 70−80% of the attached probes at Lys84 (*22*, *23*).

N-Acetyl-L-lysine was trinitrophenylated with TNBS (TNP-Lys) to serve as a spectroscopic model compound for TNP modification of S1. TNBS was added to *N*-acetyl-L-lysine in 4% $NaHCO_3$ at pH 9 at a molar ratio of 1:10. For spectroscopic measurements aliquots were taken after appropriate dilution with 20 mM HEPES buffer pH 7.

Formation of Stable S1·ADP·PA and TNP-S1·ADP·PA Complexes. S1 or TNP-Lys84-S1 (17−30 μM) was incubated in 30 mM KCl, 1 mM $MgCl_2$, 20 mM HEPES, pH 7.0, (Buffer A) at 25 °C with 0.2 mM ADP for 5 min. In the case of BeF_x-, AlF_4^--, or ScF_x-containing complexes 5 mM NaF was also present (10 mM KF for ScF_x). After that time 0.2 mM Vi, $BeCl_2$, $AlCl_3$, or $ScCl_3$ was added and the incubation continued at 25 °C for 20 min. Trap (stable complex) formation was checked by measuring Ca^{2+}-activated ATPase activity (the formation of the trap is accompanied by loss of ATPase activity (*14*)).

ATPase Assay. Ca^{2+}-activated ATPase activity (nanomoles of phosphate per milligram of S1 per minute) was calculated from the inorganic phosphate produced, measured according to Fiske and Subbarow (*35*). The reaction was performed at 25 °C on 1 mL aliquots taken at various time intervals. Incubation times were chosen so that no more than 15% of the ATP was hydrolyzed. The reaction mixture contained 1 μM S1 or TNP-modified S1, 2 mM ATP, 6 mM $CaCl_2$, 400 mM KCl, and 50 mM Tris-HCl buffer, pH 8.8, and it was incubated at 25 °C for 4 min.

Kinetics of S1 Modification. The trinitrophenylation kinetics of S1 were followed spectrophotometrically essentially as described earlier (*24*). TNBS (final concentration 100 μM) was added to 10 μM S1 in the presence or absence of nucleotides in 1 mM $MgCl_2$, 30 mM HEPES buffer, pH 7.7. The reaction was carried out in a thermostated cell of a Unikon 810 P spectrophotometer (Zurich, Switzerland) at 25 °C. The absorbance change at 345 nm was recorded, and the number of TNP groups introduced was calculated. The reaction of S1 with the TNBS has fast and slow components (*21*). In the fast reaction the trinitrophenylation of both Lys84 and the rest of S1 lysines occurs, while in the slow reaction only the rest of the S1 lysines are modified. Under the conditions of the kinetic measurements trinitrophenylation of Lys84 is essentially finished during the first 20 min of the reaction. The initial velocity of the modification of the slowly reacting lysines, υ_2, was calculated from the reaction rate 30 min after the addition of TNBS by accounting for changes in TNBS and unmodified lysine concentrations during the first 30 min of the reaction. The initial velocity of trinitrophenylation of Lys84 (υ_1) was obtained by subtracting υ_2 from the initial velocity of the overall process (υ). Since the modification of Lys84 is a pseudo-first-order reaction under the conditions of the experiment (10-fold molar excess of TNBS over S1), the first-order rate constants could be calculated from υ_1.

Circular Dichroism. Near-UV CD spectra were recorded (in Jerusalem, Israel) on a Jobin et Yvon CD 6 spectropolarimeter (Longjumeau, France) or (in Rochester, MN) on a JASCO J720 spectropolarimeter (Tokyo, Japan). Protein spectra measurements were carried out in a 10 mm thermostated cell at 20 °C containing 17 μM TNP-modified S1 in Buffer A. In addition some samples contained nucleotides and phosphate analogues as described in the various experiments. To obtain a spectrum, we recorded CD from a sample containing the S1 complex and subtracted from this a similarly recorded spectrum from an identical sample except without protein. The CD data for each wavelength were expressed as molar ellipticity, $[\Theta(\lambda)]$ (deg cm^2 $dmol^{-1}$) such that

$$[\Theta(\lambda)] = 100\Theta(\lambda)/Cl \qquad (1)$$

where $\Theta(\lambda)$ is the measured ellipticity in degrees at a given wavelength, l is the optical path length in centimeters, and C is the molar concentration of the TNP. Measurements on TNP-6p and TNP-Lys were also carried out at 20 °C.

Absorption Spectra. The absorption difference spectra were recorded in a Cary 13E spectrophotometer (Varian Instruments, Houston, TX) in 10 mm matched silica cells at 20 °C. The cells in the sample and reference position contained the same concentration of TNP-Lys84-S1 (Buffer A). To the sample cell was added 0.2 mM ADP, and the spectrum was recorded. This was followed by the addition of 5 mM NaF

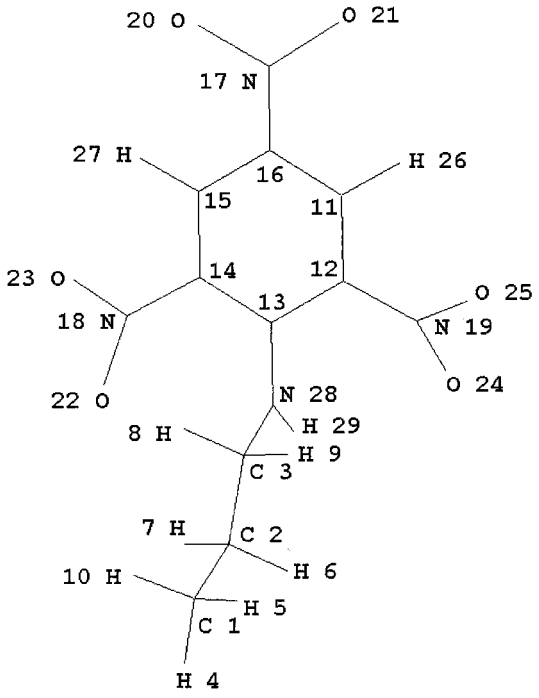

FIGURE 2: The TNP-∈-amino product molecule used in the calculation of transition monopoles. The monopoles for the two lowest energy transitions are equivalent to dipoles $\mathbf{D}_i = |\mathbf{D}_i|(\sin\theta_i\cos\phi_i,\sin\theta_i\sin\phi_i,\cos\theta_i)$ where $|\mathbf{D}_{1,2}|^2 = 9.7$, 13.0 D^2; $\theta_{1,2} = 28°$, 78°; $\phi_{1,2} = 176°$, 353°; and molecular frame $z(x)$-axis parallel to the vector pointing from atom 13(14) to atom 16(12). Calculated transition wavelength maxima for these transitions are 447 and 409 nm.

and 0.2 mM $BeCl_2$ or 0.2 mM $AlCl_3$ to both cells, and after formation of the trap, the spectrum was recorded again. Measurements on TNP-6p and TNP-Lys were also carried out at 20 °C.

Calculation of the Optical Signal. The peak absorption energy and dipole and rotary strengths for electronic transitions contributing to the visible absorption and induced CD bands of the TNP-Lys84-S1 or TNP-6p were calculated as described elsewhere (*10*). The calculation combines the two observable lowest energy transitions of the peptide amide group, the (n,π*) and (π,π*) transitions, with the observable (π,π*) transitions from the aromatic side chains and TNP modifying Lys84 in S1 or Lys3 in TNP-6p. The Coulomb potential with vacuum dielectric constant couples the transition monopoles of these excited states from interacting groups. The aromatic side chains considered include tryptophan, tyrosine, phenylalanine, and histidine (only tyrosine in TNP-6p). The position and value of the transition monopole charges for the peptide amide group (*36*) and the aforementioned side chain groups (*37*−*40*) were taken from the literature. The position and value of the transition monopole charges for the TNP were calculated as described below.

The TNP-∈-amino product shown in Figure 2 imitates TNP-modified lysine and was used to calculate the electric dipole orientations for the two lowest energy electronic transitions in the absorption spectrum for unperturbed TNP. The crystal structure gives the conformation of the TNP group (*41*, *42*). The crystal structure of Lys84 in chicken S1 (*4*) gives the initial conformation of the ∈-amino group that was subsequently energy-minimized with molecular mechanics using the MM+ force field. During energy minimization of the TNP-∈-amino product, and during all subsequently described calculations involving the conformation of TNP and the lysine side chain, the coordinates of atoms in the TNP group and the torsion angle, Ω_1, for atoms 3, 28, 13, and 12 (Figure 2) were constrained by the TNP crystal structure and the 2D-NMR structure of the model peptide (*31*), respectively. The detailed conformations of atoms 1−10 (Figure 2) have negligible impact on the calculated electric dipole orientations for the two lowest energy electronic transitions in TNP.

The semiempirical quantum mechanical method ZINDO/S with configuration interaction (CI) (*43*) was used to calculate the electric dipole orientations for the visible part of the absorption spectrum of the TNP-∈-amino product. ZINDO/S calculations were carried out in a vacuum with zero net charge and zero electronic spin in the ground state. We computed the net transition monopole charge at each atom in the molecule from the electron density matrix generated in ZINDO/S as described elsewhere (*44*). The amplitudes of the transition monopoles were normalized to reproduce the observed dipole strengths of monomeric TNP-Lys at pH 7.

Monopole charges on carbon atoms in the benzene ring of TNP were split into two equal point charges and placed equidistant from the atom along a line perpendicular to the plane of the ring in the region of the π-orbital. We used the separation distance between a carbon atom and its monopole charge suggested by Bayley et al. (*36*). Monopole charges from hydrogen atoms were summed with those from the nearest ring carbon, and monopole charges for the NO_2 groups were placed at the atomic coordinate. The net charge from the ϵ-amino group was replaced by a single charge at atom 28 (Figure 2).

The vacuum Coulomb potential accurately models the interaction between charges separated by nonpolarizable matter. In TNP-Lys84-S1 the transition monopoles separated by more than a few angstroms must interact less strongly due to the polarizability of the surrounding atoms. We account for this charge screening effect, as have others (*45*, *46*), by confining interactions to among the amide groups within 8 Å and other aromatic side chains within 14 Å of the TNP-modified lysine C_γ carbon. We showed elsewhere that these interaction distance cutoffs lead to reliable predictions for rotary strengths from S1 (*10*). In the case of the TNP-6p all possible interactions were considered.

Experiment and calculation are compared for energy, dipole strength, and rotary strength of TNP at its two lowest energy transitions having unperturbed peak absorptions at 417.1 and 353.3 nm.

RESULTS

Trinitrophenylation Kinetics. S1 without nucleotide, in the presence of ATP, ADP, and ATPγS and trapped with ADP·BeF_x, ADP·AlF_4^-, and ADP·Vi was trinitrophenylated with TNBS and the absorbance change at 345 nm monitored as a function of time during the reaction. The rapid first phase of the reaction is from modification of both Lys84 and the other lysines of S1 (*21*, *24*). This is followed by a slower second phase after completion of Lys84 trinitrophenylation when only the other lysines of S1 are reacting. All of the

Table 1: Pseudo-First-Order Rate Constants for Trinitrophenylation of Lys84 in S1 in the Absence and Presence of Nucleotides and Phosphate Analogues

addition to S1	rate constant ± SE × 10^5 (s^{-1})[a]
none	137 ± 8.6
ADP (0.2 mM)	59 ± 4.4
ATPγS (0.2 mM)	64 ± 3.9
ADP·BeF_x[b]	49 ± 2.2
ATP (4 mM)	29 ± 2.7
ADP·AlF_4^-[b]	32 ± 3.2
ADP·Vi[b]	31 ± 2.9

[a] For calculation of the rate constants and conditions of the trinitrophenylation kinetics, see Materials and Methods. SE is standard error. [b] For formation of the PA-containing complexes, see Materials and Methods.

above-mentioned ligands inhibited the rapid, but not the slower, phase of the reaction. The pseudo-first-order rate constant for modification of the fast reacting Lys84 was calculated in each case from the time course of the reaction as given in Materials and Methods. Table 1 shows the results of these calculations.

Nucleotides with and without phosphate analogues strongly inhibited the trinitrophenylation of Lys84; however, the extent of inhibition differentiates between two classes of substrate. ADP, ATPγS, and ADP·BeF_x belong to the first class with 53−64% and ATP, ADP·AlF_4^-, and ADP·Vi to the second class with 77−79% inhibition. The difference between the two classes is significant. The results indicate that the structure of S1·ADP·BeF_x in the vicinity of Lys84 is similar to the structure of ATPγS. Thus, as ATPγS (*30*), S1·ADP·BeF_x mimics the structure of M*·ATP. The finding that the inhibition caused by ADP is similar to those obtained by ATPγS and ADP·BeF_x indicates that the structure of the M*·ADP state resembles that of M*·ATP at this position. The addition of MgATP to S1 predominantly populates the M**·ADP·Pi state of the ATPase cycle (*1*). Since ADP·AlF_4^- and ADP·Vi behave like ATP regarding the inhibition of Lys84 modification, it follows that the structure of TNP-S1·ADP·AlF_4^- and TNP-S1·ADP·Vi complexes in the vicinity of Lys84 resemble the structure of the M**·ADP·Pi state.

Spectroscopic Characterization of TNP-Lys84-S1. Trinitrophenylated S1 has optical activity in the TNP absorption bands induced by the interaction of the TNP moiety with asymmetric centers on S1 (*29*). We studied whether TNP-Lys84 has a unique CD spectrum that can be distinguished from CD spectra of other TNP lysines of S1. The CD spectrum of TNP-Lys84-S1 was obtained by recording that of S1 containing 1 mole of TNP per mole of protein. The CD spectra of other S1 lysines were obtained in two ways: (1) by subtracting the spectrum of TNP-Lys84-S1 from the spectrum of S1 containing two moles of TNP per mole of S1; and (2) by carrying out trinitrophenylation of S1 in the presence of ADP, which strongly inhibits the modification of Lys84 (see ref *25* and Table 1). Figure 3 compares the CD spectrum of TNP-Lys84-S1 (○) to the spectra of other TNP lysines of S1 obtained by the two methods (□, △). Both methods give a similar CD spectrum for the trinitrophenylated residues other than Lys84. The CD spectrum of TNP-Lys84-S1 is distinct with a larger maximum at 365 nm and deeper minima at 320 and 428 nm.

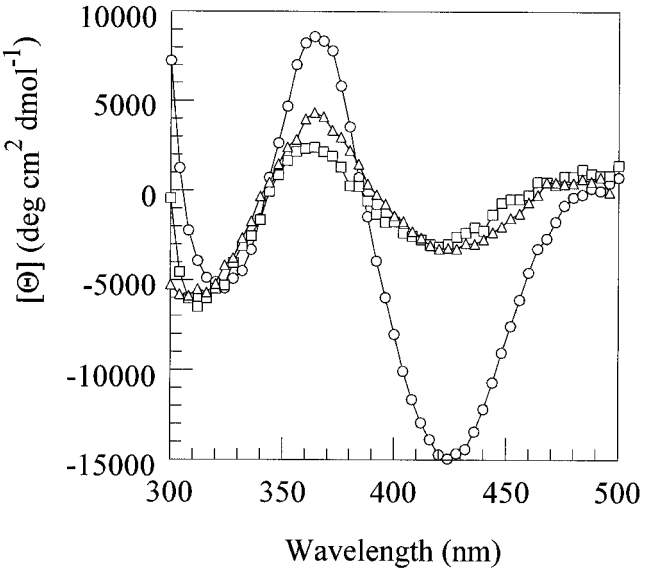

FIGURE 3: CD spectra of TNP-Lys84-S1 (○) and TNP-S1 modified at other lysines (□, △). TNP-Lys84-S1 was obtained by introducing one TNP moiety per S1. Non-Lys84-TNP-S1 spectra were obtained by recording the spectrum either of TNP-S1 modified in the presence of ADP (□) or of TNP-S1 containing two TNP per S1 minus the spectrum of TNP-Lys84-S1 (△). For conditions of the CD measurements, see Materials and Methods.

ATP and its analogues strongly affect the CD spectrum of TNP-Lys84-S1, indicating a high sensitivity of the Lys84 vicinity to conformational changes taking place in S1 during the ATPase cycle (*29*). We studied whether the spectral changes caused by analogues that mimic the M*·ATP state can be distinguished from those caused by analogues that mimic the M**·ADP·Pi intermediate of ATP hydrolysis. ATPγS (△), ADP·BeF_x (◇), and ATP (●) were used to study the CD spectrum of TNP-Lys84-S1 in the M*·ATP state (Figure 4A). In the TNP-Lys84-S1-catalyzed MgATP hydrolysis, the M*·ATP is the predominant intermediate (*28*); therefore, also in the presence of ATP the CD spectrum characteristic for the M*·ATP state is obtained. ATP and the M*·ATP mimicking analogues significantly affect the CD spectrum of TNP-Lys84-S1 (○) by causing the troughs at 320 and 428 nm to become deeper and shallower, respectively. The signal intensity at 320 nm followed the order ADP·BeF_x < ATPγS < ATP. Interestingly ADP (□) has an effect on the CD spectrum analogous to that of these compounds, showing the similarity of the S1 structures near Lys84 in the M*·ATP and M*·ADP states in agreement with the pseudo-first-order rate constants (Table 1).

ADP·AlF_4^-, ADP·Vi, and ADP·ScF_x were used to mimic the M**·ADP·Pi state. Scandium fluoride (ScF_x) also traps S1 into a stable complex (*47*), which resembles the M**·ADP·Pi state (*8*). These compounds have a dramatic effect on the CD spectrum of TNP-Lys84-S1 (○) (Figure 4B), very different from those analogues mimicking the M*·ATP state. ADP·AlF_4^- (◇) and ADP·ScF_x (△) essentially eliminate the CD spectrum from the lowest energy transitions of the TNP moiety. The 428 nm trough disappeared also with ADP·Vi (□), but the minimum at 320 nm and the maximum at 360 nm are seemingly not strongly affected; however, this is illusory since the above-mentioned maxima are due to vanadate and not to the TNP moiety (Figure 4C). Thus, the structure of S1 in the region of Lys84 differs significantly

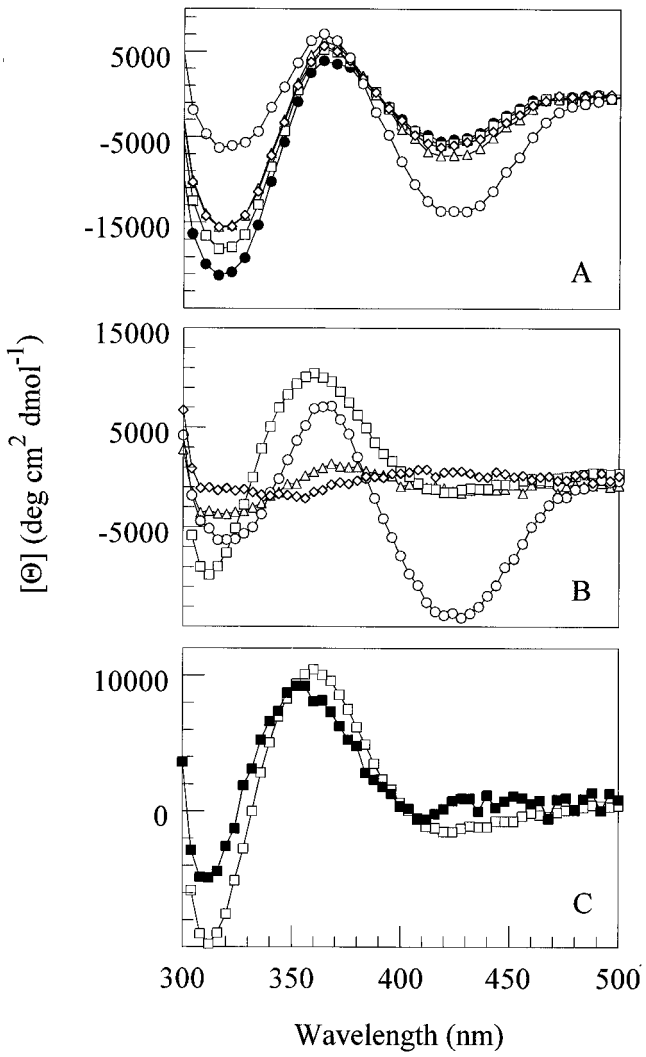

FIGURE 4: The CD spectra from TNP-Lys84-S1 in various states of the ATPase cycle. The PA-containing complexes were formed and CD spectra measured as described in Materials and Methods. (A) TNP-Lys84-S1 in the M, M*·ATP and M*·ADP states. The spectra of TNP-Lys84-S1 (○), TNP-Lys84-S1·ATPγS (△), TNP-Lys84-S1·ADP·BeF$_x$ (◇), TNP-Lys84-S1·ADP (□), and TNP-Lys84-S1 plus ATP (●) are shown. The spectra of TNP-Lys84-S1·ATPγS and TNP-Lys84-S1·ADP were recorded in the presence of 0.2 mM ATPγS and 0.2 mM ADP, respectively. TNP-Lys84-S1 plus ATP was measured with 1 mM ATP in the presence of ATP regenerating system containing 5 μM pyruvate kinase and 5 mM phosphoenol pyruvate. (B) TNP-Lys84-S1 in the M**·ADP·Pi state. The spectra of TNP-Lys84-S1 (○), TNP-Lys84-S1·ADP·AlF_4^- (◇), TNP-Lys84-S1·ADP·ScF$_x$ (△), and TNP-Lys84-S1·ADP·Vi (□) are shown. (C) Comparison of trapped ADP·Vi CD spectra from S1 (■) and TNP-Lys84-S1 (□).

in the M**·ADP·Pi intermediate from the structure of the M*·ATP, M*·ADP, and M states.

ATP and ATP analogues were shown to influence the absorption spectrum of TNP-Lys84-S1 by causing a blue shift (*29*). This spectral effect is confined to the spectrum of TNP moiety attached to Lys84 since the spectra of the rest of TNP lysines are not significantly affected by nucleotides (*29*). The spectral changes in TNP-Lys84-S1 caused by ATP and ADP are manifested in difference spectra, which showed quantitative differences while they were qualitatively similar. Since in the presence of ATP and ADP TNP-Lys84-S1 is predominantly in the M*·ATP (*28*) and M*·ADP states,

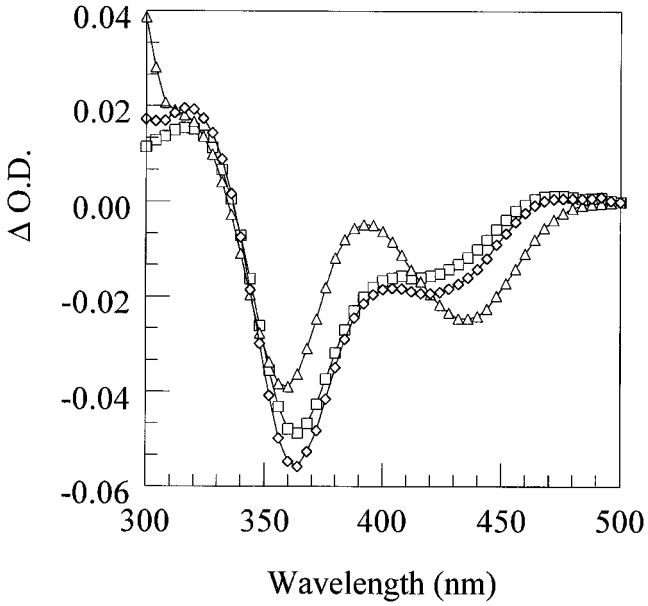

FIGURE 5: Optical density difference spectrum (Δ OD) of TNP-Lys84-S1 in the M*·ATP, M*·ADP and M**·ADP·Pi states. The spectra of TNP-Lys84-S1·ADP (□), TNP-Lys84-S1·ADP·BeF$_x$ (◇), and TNP-Lys84-S1·ADP·AlF_4^- (△) were recorded against the same concentration of TNP-Lys84-S1 in the reference cell as described in Materials and Methods.

respectively, it was of interest to study the difference spectrum also of the M**·ADP·Pi state. To get this form, we trapped TNP-Lys84-S1 with ADP·AlF_4^- (△) and compared the recorded difference spectrum with those obtained with ADP (□) and ADP·BeF$_x$ (◇) (Figure 5). The difference spectra obtained with ADP and ADP·BeF$_x$ are similar to each other and to those obtained with ATP in our previous work. These spectra have a strong minimum at 365 nm and a shoulder around 419 nm. The minimum of the ADP·BeF$_x$ spectrum at 365 nm is slightly deeper than that of the minimum of the ADP spectrum. This result is similar to those obtained in our former studies, where the trough at 365 nm in the ATP spectrum was also deeper than that in the ADP spectrum, indicating minor conformational differences in the vicinity of Lys84 between the M*·ATP and M*·ADP states. The spectrum obtained with ADP·AlF_4^- is qualitatively different from the other two spectra. It is blue-shifted relative to the ADP spectrum and has two minima at 437 and 361 nm and a maximum at 395 nm. The qualitative difference between the M**·ADP·Pi spectrum on one hand and the M*·ATP and M*·ADP spectra on the other hand supports the conclusion obtained from the measurements of the CD spectra, that is, the structure of S1 near Lys84 in the M**·ADP·Pi state differs significantly from the structure of the other states of the ATPase cycle.

Spectroscopic Characterization of Model Compounds. Figure 6 shows the extinction coefficient spectra from the model compound TNP-Lys (■) and TNP-Lys84-S1 (○) in HEPES at pH 7. Also shown is the model peptide TNP-6p in DMSO (□). The absorption spectrum from TNP-Lys as a function of concentration or pH indicates dimer or multimer formation for concentration [TNP-Lys] > ~4 μM at pH 7 (data not shown). Data in Figure 6 are for [TNP-Lys] = 1.3 μM when TNP-Lys is monomeric. Dimer or multimer formation causes a dramatic increase in the absorption band at 417 nm that is absent from the spectra in Figure 6,

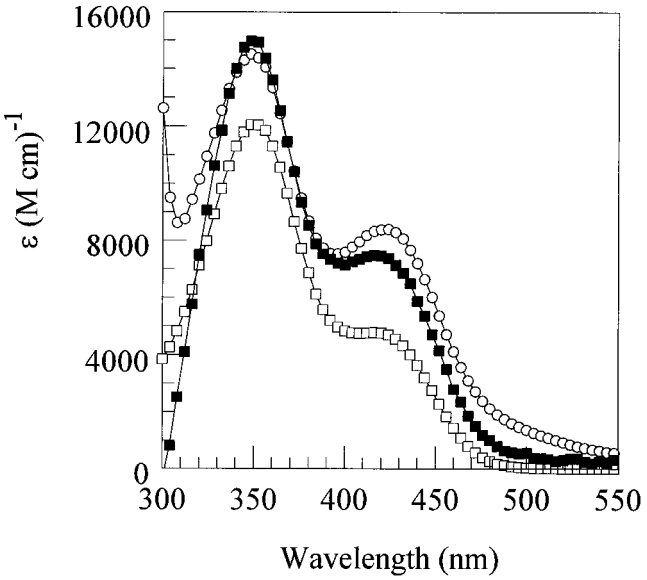

FIGURE 6: The extinction coefficient spectra from TNP-6p in DMSO (□) and TNP-Lys84-S1 (○) and TNP-Lys (■) in HEPES at pH 7.

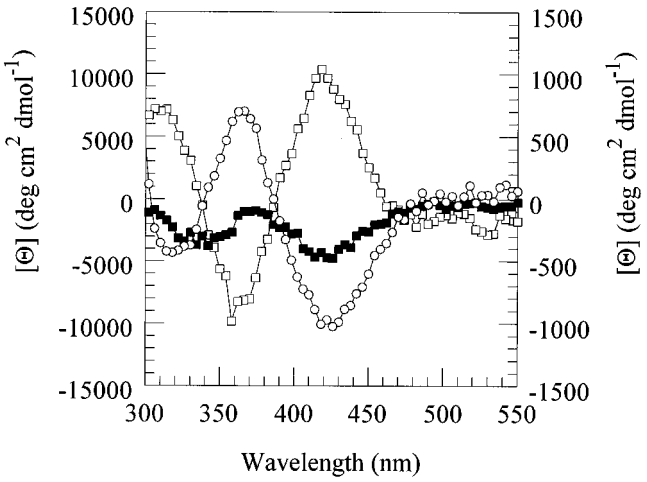

FIGURE 7: The CD extinction coefficient spectra from TNP-6p in DMSO (□) and in HEPES (■) and TNP-Lys84-S1 (○) in HEPES at pH 7. The left (right) *y*-axis is for the TNP-Lys84-S1 (TNP-6p).

indicating that the probe is monomeric when modifying S1 or the model peptide.

The CD extinction coefficient spectra from TNP-6p in DMSO (□) and in aqueous buffer (■) and from TNP-Lys84-S1 at pH 7 (○) are shown in Figure 7. Apart from a scaling factor of ∼10 the CD spectra differ only in sign. The CD spectrum from TNP-6p in aqueous buffer is similar to that from free TNP-Lys (data not shown), suggesting that TNP-6p in buffer is disordered. CD from TNP-6p in DMSO suggests that the peptide forms a well-defined static structure. 2D-NMR confirms this possibility by indicating static secondary and tertiary structure for TNP-6p with secondary structure qualitatively similar to the comparable peptide in the chicken S1 (*31*). Figure 8 shows a representative structure for TNP-6p consistent with the 2D-NMR proton distance constraints.

Optical/Structural Calculations. We calculated the rotary strength, dipole strength, and peak wavelength for the two lowest energy electronic transitions from TNP in the model peptide TNP-6p. There were no free parameters in this calculation because the TNP-6p structure was determined by 2D-NMR (*31*). The results of the calculations, performed on the structure shown in Figure 8, are summarized in Table 2. The agreement between the calculated and observed parameters demonstrates the reliability of the method.

We calculated the rotary strength, dipole strength, and peak wavelength for the two lowest energy electronic transitions from TNP in TNP-Lys84-S1 assuming the methylated chicken S1 crystallographic structure (*4*) except for the Ramachandran angles of the two glycine pivots at Gly699 (ϕ_{699},ψ_{699}) and Gly710 (ϕ_{710},ψ_{710}). These Ramachandran angles and the unknown torsion angle, Ω_2, for the bonds connecting atoms 2, 3, 28, and 13 in TNP-modified Lys84 (see Figure 2) were free parameters adjusted to minimize the difference between the observed and calculated spectroscopic parameters while avoiding atomic clashes throughout the labeled protein. Table 2 summarizes the results of the calculations including the best fitting values for ϕ_{699}, ψ_{699}, ϕ_{710}, ψ_{710}, and Ω_2.

Figure 1 shows the portion of S1 containing the interface of the catalytic and lever arm domains. The probe-binding cleft with Trp510 is separated from the TNP-Lys84 by the main α-helix of the S1. The TNP resides at the catalytic/lever arm domain interface in close proximity to Arg723. This overview represents S1 structure in the absence of nucleotide. The local TNP-S1 interactions are shown in detail in Figure 9. Panels A and B show residues within 6.5 Å of TNP in the proposed TNP-Lys84-S1 structure without nucleotide or after trapping the active site with ADP·BeF_x

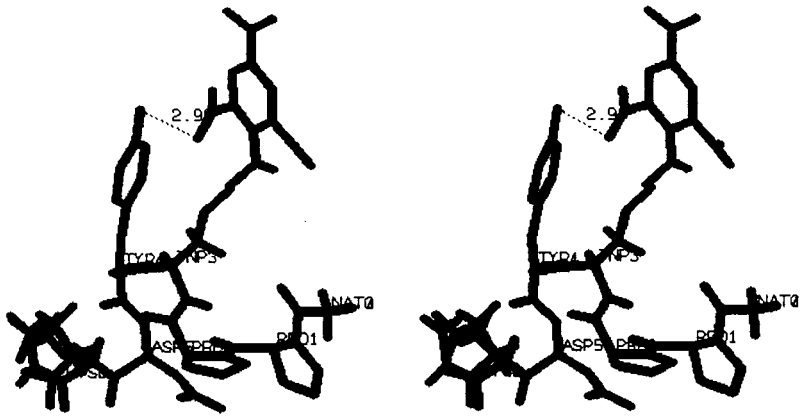

FIGURE 8: Uncrossed stereoview of a representative TNP-6p peptide structure as determined by 2D-NMR. TNP and tyrosine interact via a hydrogen bond. The group labeled NAT0 is the acetylated N-terminus.

Table 2. Structural and Optical Parameters for TNP-Lys84-S1 and TNP-6p[a]

parameter	TNP-Lys84-S1 alone	ADP·BeF_x·TNP-Lys84-S1	ADP·AlF_4^-·TNP-Lys84-S1	TNP-6p in DMSO	TNP-Lys in buffer [b]
Gly699 (ϕ_{699},ψ_{699})	(118,−4)	(108,11)	(78,28)		
Gly710 (ϕ_{710},ψ_{710})	(−79,−140)	(−79,−140)	(−85,−162)		
(Ω_1,Ω_2)	(99,−80)	(99,−95)	(99,−5)	(99,−57)	
R_1 (D−B)					
calculated	−0.109	−0.118	+0.01	+0.008	
observed	−0.099	−0.054	$\|R_1\| \leq 0.01$	+0.009	
R_2					
calculated	+0.083	+0.155	+0.00	−0.007	
observed	+0.089	+0.181	$\|R_2\| \leq 0.01$	−0.011	
D_1 (D^2)					
calculated	9.9	9.7	9.5	9.0	
observed	9.8	7.8	9.6	5.5	9.7
D_2					
calculated	12.4	12.4	11.9	12.8	
observed	5.1	7.0	3.8	10.0	13.
λ_1 (nm)					
calculated	417.3	417.3	417.3	417.4	
observed	422.0	419.5	419.0	418.5	417.1
λ_2					
calculated	353.4	353.4	353.5	353.4	
observed	360.5	353.0	348.0	354.5	353.3

[a] ϕ and ψ are Ramachandran angles for the residue numbers in the subscripts. Ω_1 and Ω_2 are torsion angles for the bonds connecting the atoms 3, 28, 13, and 12 and 2, 3, 28, and 13 in TNP-modified lysine (Figure 2). For TNP-6p in DMSO, Ω_1 and Ω_2 are fixed by 2D-NMR constraints. R_i, D_i, and λ_i correspond to the rotary strength in units of Debye-Bohr Magneton (D−B), dipole strength in Debye^2 (D^2), and peak wavelength in nanometers (nm) of the lowest (1) and next to lowest (2) energy electronic transitions of TNP for calculated and observed values. [b] TNP-Lys and TNP-6p in HEPES, pH 7, were tried as model compounds for TNP unperturbed by side chain interactions (in HEPES near-UV CD detects no tertiary structure in TNP-6p, see Figure 7). The observed peak energies varied slightly, and observed dipole strengths ranged from 5.8 to 9.7 D^2 for D_1 and from 5.9 to 13.0 D^2 for D_2 for these compounds. All model compounds gave identical values for the best fitting free parameters ϕ_{699}, ψ_{699}, ϕ_{710}, ψ_{710}, and Ω_2. The calculated D_2 for TNP-Lys84-S1 overestimates observed values because the unperturbed dipole strength (assumed to be 13.0 D^2) is too large to be compensated by any available protein-TNP interaction causing hypochromicity in this band. This discrepancy could be from the systematic underestimate of the observed D_2 because this transition appears as a shoulder on the much larger protein absorption band, making its dipole strength difficult to accurately separate from the protein contribution. Estimates of R_2 for TNP-Lys84-S1 are not sensitive to this difficulty because the protein CD spectrum is relatively much less intense in this wavelength range.

or ADP·AlF_4^- to imitate the M*ATP or M**·ADP·Pi conformations in S1. In all cases, Tyr85 directly perturbs the spectroscopic signal from TNP by its polarity and polarizability. Tyr85 and/or Arg723 play indirect roles in this spectroscopy by affecting probe mobility through their interaction with TNP-NO_2 groups.

In S1 without nucleotide (Figure 9A, green), Tyr724 perturbs TNP spectroscopy by its proximity and Arg723 interacts electrostatically with a TNP-NO_2 group to constrain independent probe movement. Swiveling exclusively at Gly699, caused by trapping the active site of TNP-Lys84-S1 with ADP·BeF_x to imitate the M*·ATP conformation in S1, directly perturbs the spectroscopic signal from TNP by slightly altering the relative position of the Tyr724 and other local backbone amide groups on the moving domain (Figure 9A, blue). The relative position of Tyr85 and TNP is also slightly altered by the independent movement of the probe further perturbing the spectroscopic signal from TNP. The Arg723-TNP ionic interaction occurs with a different TNP-NO_2 group than in the no nucleotide conformation but remains substantial. Not shown in Figure 9A is a repulsive Glu776-TNP interaction in the M*·ATP conformation (blue) that is not expected to overpower the Arg723-TNP attraction since solvent or minor side chain rearrangement can mitigate its strength. We find that the conformation of S1 in the neighborhood of Lys84 is similar in the M and M*·ATP states, as implied qualitatively by the modest perturbation of the M conformation spectroscopic signature upon formation of the M*·ATP intermediate.

Swiveling at Gly710 and Gly699, caused by trapping the active site of TNP-Lys84-S1 with ADP·AlF_4^- to imitate the M**·ADP·Pi conformation, directly perturbs the spectroscopic signal from TNP by radically altering the relative position of the Tyr724 and other local backbone amide groups on the moving domain (Figure 9B). The relative position of Tyr85 and TNP is also altered by the independent movement of the probe further perturbing the spectroscopic signal from TNP. The glycine swiveling abolishes the Arg723-TNP ionic interaction, but a hydrogen bond between Tyr85 and TNP could serve to immobilize TNP in this configuration. The Glu777-TNP ionic interaction is weaker and repulsive as shown but is positioned to drive the TNP group into closer interaction with Tyr85. The Glu777-TNP distance indicates that the lever arm remains near to the TNP but not as close as in panel A. Unlike Figure 9A, Arg723 and Tyr724 in Figure 9B are not, but the other residues shown are, within 6.5 Å of TNP. We find that the conformation of S1 in the neighborhood of Lys84 is radically altered by formation of the M**·ADP·Pi state as implied qualitatively by the radical perturbation of the M conformation spectroscopic signature upon formation of the M**·ADP·Pi intermediate.

The swiveling at Gly699 and Gly710 causes collision of TNP and the lever arm peptide backbone. Figure 9C shows the intersection of lever arm residues with TNP modifying Lys84 at a point in the lever arm trajectory during the M*·ATP → M**·ADP·Pi transition. The lever arm/TNP collision occurs only if movement at Gly710 precedes that at Gly699 during the M*·ATP → M**·ADP·Pi transition.

The observed 10-fold reduction in the TNP CD signal strength from TNP-Lys84-S1 upon formation of the M**·ADP·Pi from the M conformation could be due either to the formation of the static local conformation of TNP in S1

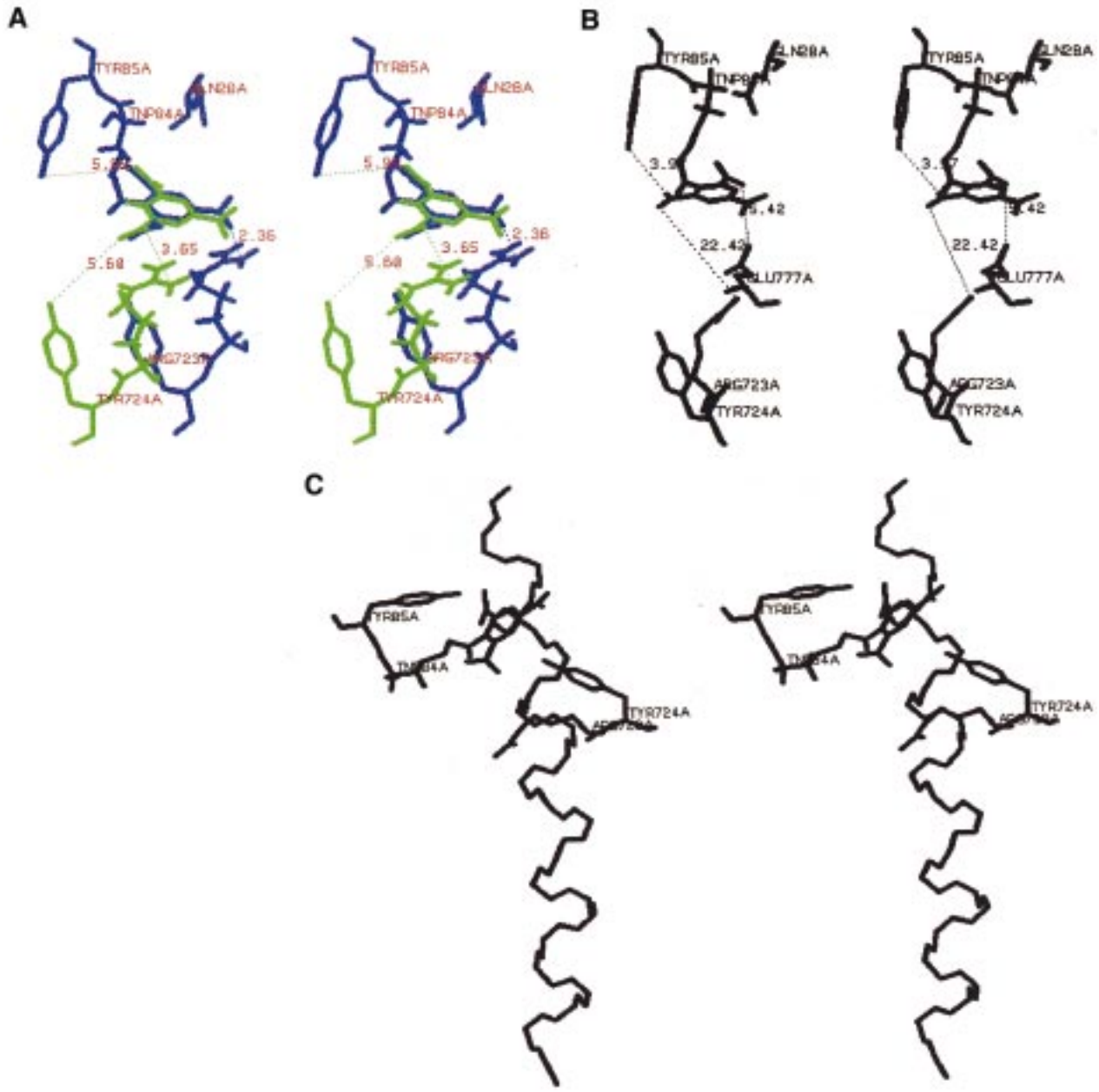

FIGURE 9: Uncrossed stereoviews of myosin structure in the vicinity of Lys84 for the following: TNP-Lys84-S1 in green and ADP·BeF_x·TNP-Lys84-S1 in blue (A), ADP·AlF_4^-·TNP-Lys84-S1 (B), and TNP-Lys84-S1 during transition between ADP·BeF_x and ADP·AlF_4^--induced structures (C). In panel C the C-terminus of the protein is toward the bottom of the figure.

shown in Figure 9B, or to an increase in independent probe mobility and the ensemble averaging of signals. The TNP-Tyr85 interaction in S1, in the absence of other constraints from the protein matrix, likely constrains probe mobility just as does the equivalent interaction in TNP-6p (Figure 8). However, we do not exclude the possibility that increased probe mobility causes some of the decrease in the CD signal when TNP-Lys84-S1 assumes the M**·ADP·Pi state.

DISCUSSION

Trapped or unhydrolyzable nucleotide analogues elucidate the molecular mechanism of energy transduction in myosin provided that they can reproduce the transient structures in S1 that accompany ATP hydrolysis. In the past, using spectroscopic techniques that probed critical regions of S1 in solution, we found correlations suggesting a relationship between the transient and analogue-induced states of the protein (*19*, *20*). Here we again investigate the relationship between various nucleotide analogue-induced and transient intermediate structures with a probe at an interface of the catalytic and lever arm domains in S1. As before, the analogue-induced structures qualitatively resemble the ATPase intermediates, judging from spectroscopic signals from the probe. We further interpret these results using methods to surmise protein structure from the spectroscopic signals to identify key features of S1 conformation change during energy transduction.

Lys84, located in the catalytic domain of S1 at an interface with the lever arm (Figure 1), is selectively trinitrophenylated by TNBS. The spectroscopic signature of the bound probe, most notably the CD signal induced in its absorption band, senses and distinguishes various nucleotides or nucleotide

analogues occupying the active site. The reaction rate of Lys84 in native S1 similarly senses and distinguishes various bound nucleotides or nucleotide analogues. The induced CD and reaction rates in the presence of MgATP characterize the M*·ATP and M**·ADP·Pi intermediates of ATP hydrolysis, respectively. This is because M*·ATP is the predominant intermediate in TNP-Lys84-S1-catalyzed MgATP hydrolysis so that the CD spectrum from TNP-Lys84-S1 in the presence of ATP is characteristic to the M*·ATP state, while M**·ADP·Pi is the predominant intermediate in S1-catalyzed MgATP hydrolysis so that the reaction rate of Lys84 in the presence of ATP is characteristic to the M**·ADP·Pi state.

We measured absorption and CD spectra from TNP-Lys84-S1 alone and in the presence of MgATP or other nucleotides or nucleotide analogues. All of the observed TNP spectroscopic signatures fall into one of three categories, one from TNP-Lys84-S1 in the absence of nucleotide, another associating ATPγS and ADP·BeF_x with the M*·ATP conformation because of the shared characteristics with TNP-Lys84-S1 in the presence of ATP (Figure 4A), and a third associating ADP·AlF_4^-, ADP·Vi, and ADP·ScF_x with the M**·ADP·Pi conformation by default (Figure 4B).

The conclusions drawn from the spectroscopy are confirmed for each analogue by the pseudo-first-order rate constants for modification of Lys84 (Table 1). The rate constants also fall into three categories, the fastest rate for S1 in the absence of nucleotide, the slowest rate for S1 in the presence of MgATP or when trapped by ADP·$AlF^-{}_4$ or ADP·Vi, and an intermediate rate for S1 in the presence of MgATPγS or when trapped by ADP·BeF_x. In disagreement with these results, rates for trinitrophenylation of Lys84 at high ionic strength (0.5 M KCl) are similar for S1 trapped with ADP·BeF_x or in the presence of ATP but smaller than that for ADP·AlF_4^--trapped S1 (*48*). Our spectroscopic and reaction rate data, taken together and notwithstanding the results at high ionic strength, confirm earlier work about the ability of the trapped nucleotide analogues to induce structural change in S1 mimicking those produced transiently by ATP hydrolysis.

The spectroscopy of TNP-Lys84-S1 shows very large contrast among signals for the M, M*·ATP, and M**·ADP·Pi conformations making them suitable for further analysis by model calculations. We compute probe CD and absorption signals using theoretical methods capable of quantifying the perturbed spectroscopic properties of ground-state transitions in TNP caused by changes in interactions between the probe and surrounding protein residues. The two glycine pivots at Gly699 and Gly710, already implicated in the mechanism of energy transduction (*5*, *6*, *11*), generate the local structural changes.

The model calculations giving CD and absorption signals from atomic structure are based on a number of approximations and assumptions discussed in the original literature (*36*, *49*). We investigated the reliability of these calculations by applying them first the TNP-6p model system with known structure. Table 2 summarizes the parametrization of the spectroscopic signals from TNP-6p in DMSO and shows that our calculation predicts the observed spectral parameters given the peptide structure. Naturally this exercise gives us confidence in our findings in the reverse direction, where, given the spectroscopic parameters, we infer structure. The reverse problem is under-determined, but information provided by the S1 crystal structure (*4*) and the identification of Gly699 and Gly710 as the pivots generating conformational change in energy transduction (*5*, *6*, *10*, *11*) give sufficient supplementary constraints to make the calculation feasible and informative.

The panels of Figure 9 show the key residues making up the neighborhood of TNP-modified Lys84 in S1. The M (green) conformation (Figure 9A) has an immobilized probe most likely because of the Arg723-TNP interaction. Both Lys84 and Arg723 are conserved residues in the myosin family, suggesting that they could have functional significance (*50*). This structure differs from the crystallographic structure of skeletal S1 (*4*) only in the Ramachandran angles for the two swivels at Gly699 and Gly710. The M structure of Figure 9A, similar to that suggested previously from various spectroscopic measurements of the probe-binding cleft conformation and a structural model using only the Gly699 pivot (*10*), uses swiveling at Gly710 to better accommodate the new data from TNP-Lys84-S1.

The proposed M*·ATP (blue) structure differs from the proposed M structure due to swiveling only at Gly699 (Figure 9A). The M*·ATP structure is inconsistent with the smooth muscle crystallographic coordinates for ADP·BeF_x-trapped S1 (*11*). The crystal structures of smooth muscle S1 when trapped with ADP·BeF_X or ADP·AlF_4^- have been reported as essentially identical, unlike implications from solution studies on skeletal S1 (*19*, *20*) and the crystal structures of the recombinant S1Dc (*15*, *16*). The dissimilar results could be from differences among the three kinds of S1 studied or from properties of the ADP·BeF_X analogue. Recent work comparing smooth and skeletal muscle myosin active site conformations shows that these molecules respond differently to trapping by the nucleotide analogues (*18*). There it is shown that the active site conformation of skeletal myosin distinguishes the trapped ADP·BeF_X and ADP·AlF_4^- analogues while smooth muscle myosin fails to distinguish these trapped analogues such that both induce an active site conformation similar to that in ADP·AlF_4^--trapped skeletal myosin. In other work, ^{19}F NMR spectroscopy suggests that ADP·BeF_X-trapped S1 exists in more than one conformation, perhaps mimicking both M*·ATP and M**·ADP·Pi (*51*). If so, the smooth muscle S1 crystal might select the ADP·BeF_X conformer mimicking the M** state, ensuring similarity between the trapped ADP·AlF_4^- and ADP·BeF_X smooth muscle S1 structures. Why the crystal of the ADP·BeF_X·S1Dc does not similarly prefer the M** conformer is unknown; however, another crystal structure of S1Dc·ADP·BeF_x (*52*) was reported as similar to that obtained previously for S1Dc·Vi (*16*). As S1Dc·ADP·Vi mimics the M** conformer, it appears that crystallization conditions determine the preference for either the M* or M** conformer.

The proposed M**·ADP·Pi structure in Figure 9B differs from the proposed M structure in Figure 9A due to swiveling at both Gly710 and Gly699. The M*·ATP → M**·ADP·Pi transition also involves swiveling at both Gly710 and Gly699 but with the larger conformation change at Gly710. This M**·ADP·Pi structure is consistent with the smooth muscle crystallographic coordinates for ADP·AlF_4^--trapped S1 (*11*) but inconsistent with that suggested previously from various

spectroscopic measurements of the probe-binding cleft conformation and a structural model using only the Gly699 pivot (*10*). Superposition of ADP·AlF_4^--trapped smooth and skeletal muscle S1 structures, where skeletal S1 structure without nucleotide is swiveled at Gly710 and Gly699 using the Ramachandran angles given in Table 2, shows a high degree of similarity in the catalytic and lever arm regions of the proteins. Most importantly, alignment of the catalytic regions produces similar positioning of the lever arm in the smooth and skeletal S1. However, the M**·ADP·Pi structure of Figure 9B has a distorted probe-binding cleft conformation (not shown) that is inconsistent with our findings on changes in the collisional quenching of Trp510 during ATP hydrolysis (*7*, *8*). We believe that conformation change in the catalytic domain, not accounted for by swiveling at Gly710 and Gly699, affects the probe-binding cleft causing it to close during ATP hydrolysis. This effect is displayed in the smooth muscle M**·ADP·Pi conformation (*11*), where the probe-binding cleft is slightly more closed than that in skeletal S1 without nucleotide (*4*). A more definitive explanation of this discrepancy should follow from the crystallographic structure of one type of S1 (either smooth or skeletal) determined in both the M and the M*·ATP or M**·ADP·Pi conformations.

Figure 9C shows the intersection of the lever arm with TNP modifying Lys84 at a point in the lever arm trajectory during the M*·ATP → M**·ADP·Pi transition. The path of the lever arm movement produced by the glycine swivels is a function of the extent of swiveling and the order in which swiveling occurs. The extent of swiveling is the difference in the Ramachandran angles in the final from that in the initial configuration. The order pertains to whether Gly710 or Gly699 swivels first and, within one glycine residue, which Ramachandran angle, ϕ or ψ, changes first. The ordering of rotational movement producing Figure 9C has Gly710 swiveling first in the M*·ATP → M**·ADP·Pi transition. Our data did not the specify an order for the Ramachandran angles within either glycine residue. This swiveling order satisfies all of the spectroscopic constraints and provides an explanation for the effect of trinitrophenylation on ATPase.

The probe modification of Lys84 causes activation of the Mg^{2+}-ATPase of S1. The structural consequences of ATP hydrolysis in the neighborhood of Lys84 at the interface of catalytic and lever arm domains, indicated in Figure 9, has the lever arm colliding with the foreign TNP group during the formation of M**·ADP·Pi. Without TNP the domains in S1, moving in identical trajectory, do not intersect, suggesting that the TNP collision destabilizes the M**·ADP·Pi transient by disturbing the normally stabilizing interaction of residues at or near to Lys84. The probe modification of Cys707 also causes activation of the Mg^{2+}-ATPase of S1, and the probe-binding cleft containing Cys707 has a similar interface of catalytic and lever arm residues (Figure 1) wherein formation and stabilization of the M**·ADP·Pi conformation may likewise involve the close proximity or near collision of residues at the interface (*10*). We propose that the lever arm/catalytic domain interfaces near Lys84 and Cys707 are made up of residues on both sides on the interface that interact favorably to stabilize M**·ADP·Pi. If this is the case, then the mutation of residues on the lever arm domain but near Lys84 (for instance at or near Arg723) could likewise destabilize this rate-limiting step in ATPase. The mutation of residues in this vicinity occurs in hypertrophic cardiomyopathy (for instance at Lys721 or Arg725 (*53*, *54*)), suggesting that destabilizing M**·ADP·Pi in the absence of actin could be a cause of heart failure in this disease. Actin binding to native MgATP·S1 also activates Mg^{2+}-ATPase, raising the possibility that it too perturbs the favorable interaction of residues at one or both of these interfaces.

Simultaneous with Mg^{2+}-ATPase activation is K^+-EDTA ATPase inhibition after modification of Lys84 or Cys707. In K^+-EDTA ATPase, removal of the divalent cation from the native protein destabilizes substrate binding at the active site but supports rapid ATP hydrolysis in the presence of monovalent cation (*55*). TNP-modified S1 resists the M*·ATP → M**·ADP·Pi transition by intersecting the lever arm as shown in Figure 9C. This increased internal resistance may be sufficient to stop lever arm movement driven by the weakly bound substrate and halt or subvert (by dissociating substrate) K^+-EDTA ATPase. The more robust Mg^{2+}-ATPase, with a firmly bound substrate, delivers sufficient energy to the S1 to overwhelm the higher internal resistance in the TNP-Lys84-S1 motor. An equivalent mechanism may be at work, causing changes in ATPases due to Cys707 modification. This notion is supported by the observation that probes of various shapes and sizes modifying Cys707 have the same qualitative effect, that is, to activate Mg^{2+}-ATPase and inhibit K^+-EDTA ATPase, but differing quantitative effects that are characteristic to each probe.

The structures of Figure 9 also suggest an explanation for the anomalous p*K* of Lys84 causing its higher reactivity, in the absence of nucleotide, compared to the other exposed lysine residues in S1 (*24*). The side chain p*K* of Arg exceeds that of Lys such that the close proximity of Arg723 and Lys84 in the absence of nucleotide could deprotonate the Lys side chain ϵ-amino group. Formation of the M**·ADP·Pi conformation in S1 removes Arg723 from the immediate neighborhood of Lys84 and dramatically lowers reactivity by allowing Lys84 to accept a proton. The intermediate reactivity of Lys84 in the M*·ATP conformation may be from the modest movement of Arg723 upon formation of the M*·ATP state, causing misalignment of atoms participating in the proton exchange (*56*). Cardiac S1 also possesses a reactive lysyl residue (RLR) and an arginine residue in the equivalent positions to Lys84 and Arg723 in chicken skeletal myosin; however, Tyr85 is replaced by Phe. Cardiac RLR reaction rates are 2−3-fold less than that of skeletal RLR but still anomalously higher than the other exposed lysines (*57*). This observation implies a role for Tyr85 in the anomalous behavior of RLR, possibly as an additional proton acceptor from Lys84. Other structural or functional differences in cardiac myosin may also prevent Arg-RLR proximity and alignment in this system.

The proposed M, M*·ATP, and M**·ADP·Pi structures in Figure 9 support the notion that passage through these intermediates causes correlated movement of the lever arm and conformational change at the probe-binding cleft. More specifically, swiveling principally at Gly699 accompanies the structural transition M → M*·ATP, and swiveling principally at Gly710 accompanies the structural transition M*·ATP → M**·ADP·Pi. This partitioning of the conformation change in S1 during ATP hydrolysis possibly parallels

that occurring during force generation, where, after strong binding to the actin filament, phosphate release M**·ADP·Pi → M*·ADP + Pi then ADP release M*·ADP → M + ADP is accompanied by inverse swiveling at Gly710 then Gly699, respectively. This scenario explains the similarity of the spectroscopic signatures of TNP-Lys84-S1 in the M*·ADP and M*·ATP states (Figure 4A) and why probes bound to SH1 detect the binding of MgADP to fibers in rigor (*58*). This scenario is also consistent with the observed partitioning of cross-bridge attitude changes during force production into torsional and polar rotations, where the axes of rotations are parallel and perpendicular to the long dimension of the S1, respectively (*59*).

We have used TNP as a site-specific structural perturbant of S1 and as a chiral reporter group for the effect of Lys84 modification on S1 structure. This dual role for TNP enhances its significance for investigating myosin's energy transduction mechanism and suggests that, subsequently, other optically active and structurally perturbative probes of S1 may be productive determinants of the mechanism of energy transduction. This method of investigation turns a normally negative aspect of probe modification of a protein, that is, the probes non-negligible impact on function, into an investigative tool.

Summarizing, the CD and absorption spectra from TNP modifying RLR in skeletal S1 and the pseudo-first-order rate constants for RLR modification in native S1 sense and distinguish the M, M*·ATP, and M**·ADP·Pi states of the ATPase intermediates defined in Scheme 1. Trapped phosphate analogues emulated these observable characteristics of the protein, reaffirming a structural correlation between ATPase intermediates and static structures induced by trapped PA's. Model calculations, calibrated using a small peptide of known structure containing TNP, were used to further study the transient structures of S1 during ATPase. Calculation of the peak energy, dipole strength, and rotary strength from the two lowest energy transitions of TNP in TNP-Lys84-S1, using the skeletal S1 crystallographic structure and pivots at Gly699 and Gly710 to model conformation changes during energy transduction, account for the spectroscopic signals observed from TNP-Lys84-S1 in conformations induced by the PA's to imitate the M, M*·ATP, and M**·ADP·Pi states. The model calculations indicate lever arm trajectory during ATPase and suggest that interactions between residues at the interface of the lever arm and catalytic domains near Lys84 stabilize the rate-limiting ATPase intermediate state. TNP is a site-specific structural perturbant of S1 and a chiral reporter group for the effect of Lys84 modification on S1 structure. As such, TNP-Lys84-S1 is equivalent to a genetically engineered mutant with intrinsic sensitivity to structure local to the modified residue.

ACKNOWLEDGMENT

We thank Mrs. S. P. Garamszegi for technical assistance and Dr. D. McCormick from the Mayo Protein Core Facility for the synthesis of the TNP-6p.

REFERENCES

1. Bagshaw, C. R., and Trentham, D. R. (1974) *Biochem. J. 141*, 331−349.
2. Huxley, H. E. (1969) *Science 164*, 1356−1366.
3. Huxley, A. F., and Simmons, R. M. (1971) *Nature 233*, 533−538.
4. Rayment, I., Rypniewski, W. R., Schmidt-Base, K., Smith, R., Tomchick, D. R., Benning, M. M., Winkelmann, D. A., Wesenberg, G., and Holden, H. M. (1993) *Science 261*, 50−58.
5. Kinose, F., Wang, S. X., Kidambi, U. S., Moncman, C. L., and Winkelmann, D. A. (1996) *J. Cell Biol. 134*, 895−909.
6. Patterson, B., Ruppel, K. M., Wu, Y., and Spudich, J. A. (1997) *J. Biol. Chem. 272*, 27612−27617.
7. Park, S., Ajtai, K., and Burghardt, T. P. (1996) *Biochim. Biophys. Acta 1296*, 1−4.
8. Park, S., Ajtai, K., and Burghardt, T. P. (1997) *Biochemistry 36*, 3368−3372.
9. Park, S., Ajtai, K., and Burghardt, T. P. (1996) *Biophys. Chem. 63*, 67−80.
10. Burghardt, T. P., Garamszegi, S. P., Park, S., and Ajtai, K. (1998) *Biochemistry 37*, 8035−8047.
11. Dominguez, R., Freyzon, Y., Trybus, K. M., and Cohen, C. (1998) *Cell 94*, 559−571.
12. Goodno, C. C. (1979) *Proc. Natl. Acad. Sci. U.S.A. 76*, 2620−2624.
13. Phan, B., and Reisler, E. (1992) *Biochemistry 31*, 4787−4793.
14. Werber, M. M., Peyser, Y. M., and Muhlrad, A. (1992) *Biochemistry 31*, 7190−7197.
15. Fisher, A. J., Smith, C. A., Thoden, J. B., Smith, R., Sutoh, K., Holden, H. M., and Rayment, I. (1995) *Biochemistry 34*, 8960−8972.
16. Smith, C. A., and Rayment, I. (1996) *Biochemistry 35*, 5404−5417.
17. Ponomarev, M. A., Timofeev, V. P., and Levitsky, D. I. (1995) *FEBS Lett. 371*, 261−263.
18. Maruta, S., Henry, G. D., Ohki, T., Kambara, T., Sykes, B. D., and Ikebe, M. (1998) *Eur. J. Biochem. 252*, 520−529.
19. Peyser, Y. M., Ajtai, K., Werber, M. M., Burghardt, T. P., and Muhlrad, A. (1997) *Biochemistry 36*, 5170−5178.
20. Phan, B. C., Peyser, Y. M., Reisler, E., and Muhlrad, A. (1997) *Eur. J. Biochem. 243*, 636−642.
21. Kubo, A., Tokura, S., and Tonomura, Y. (1960) *J. Biol. Chem. 235*, 2835−2839.
22. Mornet, D., Pantel, P., Bertrand, R., Audemard, E., and Kassab, R. (1980) *FEBS Lett. 117*, 183−188.
23. Hozumi, T., and Muhlrad, A. (1981) *Biochemistry 20*, 2945−2950.
24. Muhlrad, A., and Takashi, R. (1981) *Biochemistry 20*, 6749−6754.
25. Tonomura, Y., Yoshimura, J., and Onishi, T. (1963) *Biochim. Biophys. Acta 78*, 698−700.
26. Kitagawa, S., Yoshimura, J., and Tonomura, Y. (1961) *J. Cell Biol. 236*, 902−906.
27. Fabian, F., and Muhlrad, A. (1968) *Biochim. Biophys. Acta 162*, 596−603.
28. Muhlrad, A. (1983) *Biochemistry 22*, 3653−3660.
29. Muhlrad, A. (1977) *Biochim. Biophys. Acta 493*, 154−166.
30. Goody, R. S., and Hofman, W. (1980) *J. Muscle Res. Cell Motil. 1*, 101−115.
31. Burghardt, T. P., Juranic, N., Macura, S., Muhlrad, A., and Ajtai, K. (1999) (manuscript in preparation).
32. Tonomura, Y., Appel, P., and Morales, M. (1966) *Biochemistry 5*, 515−521.
33. Weeds, A. G., and Taylor, R. S. (1975) *Nature 257*, 54−56.
34. Okuyama, T., and Satake, K. (1960) *J. Biochem. 47*, 454−462.
35. Fiske, C. H., and Subbarow, Y. (1925) *J. Biol. Chem. 66*, 375−400.
36. Bayley, P. M., Nielsen, E. B., and Schellman, J. A. (1969) *J. Phys. Chem. 73*, 228−243.
37. Goux, W. J., Radesch, T. R., and Hooker, T. M. (1976) *Biopolymers 15*, 977−997.
38. Goux, W. J., Cooke, D. B., Rodriguez, R. E., and Hooker, T. M. (1974) *Biopolymers 13*, 2315−2329.
39. Hsu, M. (1970) Ph.D. Thesis, University of Illinois, Urbana, IL, pp 1−145.

40. Grebow, P. E., and Hooker, T. M. (1975) *Biopolymers 14*, 871−881.
41. Dudis, D. S., and Gilardi, R. (1990) *Acta Crystallogr., Sect. C 46*, 648−650.
42. George, C., and Dudis, D. S. (1990) *Acta Crystallogr., Sect. C 46*, 650−652.
43. Anderson, W. P., Edwards, W., and Zerner, M. C. (1986) *Inorg. Chem. 25*, 2728−2732.
44. Ajtai, K., Dai, F., Park, S., Zayas, C. R., Peyser, Y. M., Muhlrad, A., and Burghardt, T. P. (1998) *Biophys. Chem. 71*, 205−220.
45. Strickland, E. H. (1972) *Biochemistry 11*, 3465−3474.
46. Goux, W. J., and Hooker, T. M. (1980) *J. Am. Chem. Soc. 102*, 7080−7087.
47. Gopal, D., and Burke, M. (1995) *J. Biol. Chem. 270*, 19282−19286.
48. Maruta, S., Homma, K., and Ohki, T. (1998) *J. Biochem. 124*, 578−584.
49. Tinoco, I. (1960) *J. Chem. Phys. 33*, 1332−1338.
50. Mornet, D., Bonet, A., Audemard, E., and Bonicel, J. (1989) *J. Muscle Res. Cell Motil. 10*, 10−24.
51. Henry, G. D., Maruta, S., Ikebe, M., and Sykes, B. D. (1993) *Biochemistry 32*, 10451−10456.
52. Holmes, K. C. (1998) A molecular model for muscle contraction. *European Muscle Conference 27*, C1.
53. Rayment, I., Holden, H. M., Sellers, J. R., Fananapazir, L., and Epstein, N. D. (1995) *Proc. Natl. Acad. Sci. U.S.A. 92*, 3864−3868.
54. Roberts, R., Marian, A. J., and Bachinski, L. (1998) *J. Cardiac Failure 2*, S87−S95.
55. Lymn, R. W., and Taylor, E. W. (1970) *Biochemistry 9*, 2975−2983.
56. Scheiner, S. (1985) *Acc. Chem. Res. 18*, 174−180.
57. Muhlrad, A., Srivastava, S., Hollosi, G., and Wikman-Coffelt, J. (1981) *Arch. Biochem. Biophys. 209*, 304−313.
58. Borejdo, J., Assulin, O., Ando, T., and Putnam, S. (1982) *J. Mol. Biol. 158*, 391−414.
59. Ajtai, K., Toft, D. J., and Burghardt, T. P. (1994) *Biochemistry 33*, 5382−5391.

BI990149R